

Tuhin Dey ⁽¹⁾; Augustus W. Arbogast ⁽¹⁾; Qian Meng ⁽¹⁾; Md. Shamim Reza ⁽¹⁾; Aaron J. Muhowski ⁽¹⁾; Joshua J. P. Cooper ⁽¹⁾; Erdem Ozdemir; Fabian U. Naab ⁽¹⁾; Thales Borrely ⁽¹⁾; Jonathan Anderson ⁽¹⁾; Rachel S. Goldman ⁽¹⁾; Daniel Wasserman ⁽¹⁾; Seth R. Bank ⁽¹⁾; Mark W. Holtz ⁽¹⁾; Edwin L. Piner ⁽¹⁾; Mark A. Wistey ⁽²⁾

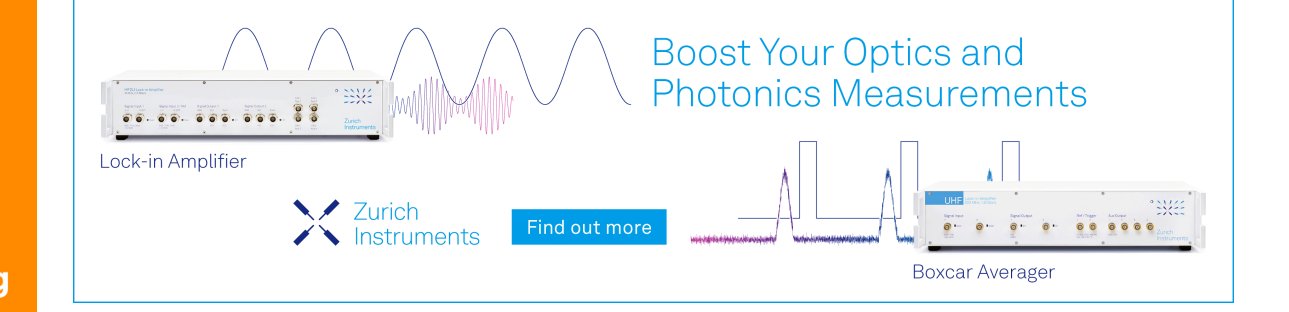


J. Appl. Phys. 134, 193102 (2023) https://doi.org/10.1063/5.0173429





Export Citation





Cite as: J. Appl. Phys. 134, 193102 (2023); doi: 10.1063/5.0173429

Submitted: 22 August 2023 · Accepted: 24 October 2023 ·

Published Online: 15 November 2023







Tuhin Dey,¹ D Augustus W. Arbogast,² D Qian Meng,³ D Md. Shamim Reza,¹ D Aaron J. Muhowski,^{3,a)} D Joshua J. P. Cooper,⁴ D Erdem Ozdemir,⁴ Fabian U. Naab,⁵ D Thales Borrely,⁶ D Jonathan Anderson,² Rachel S. Goldman,^{4,6} D Daniel Wasserman,³ Seth R. Bank,³ Mark W. Holtz,^{1,2} D Edwin L. Piner,^{1,2} D and Mark A. Wistey^{1,2,b)}

AFFILIATIONS

- ¹Materials Science, Engineering, and Commercialization Program, Texas State University, San Marcos, Texas 78666, USA
- Department of Physics, Texas State University, San Marcos, Texas 78666, USA
- ⁵Department of Electrical and Computer Engineering, University of Texas Austin, Austin, Texas 78758, USA
- Department of Materials Science and Engineering, University of Michigan, Ann Arbor, Michigan 48109, USA
- ⁵Michigan Ion Beam Laboratory, University of Michigan, Ann Arbor, Michigan 48109, USA

ABSTRACT

GeSnC alloys offer a route to direct bandgap semiconductors for CMOS-compatible lasers, but the use of CBr₄ as a carbon source was shown to reduce Sn incorporation by 83%–92%. We report on the role of thermally cracked H in increasing Sn incorporation by 6x–9.5x, restoring up to 71% of the lost Sn, and attribute this increase to removal of Br from the growth surface as HBr prior to formation of volatile groups such as SnBr₄. Furthermore, as the H flux is increased, Rutherford backscattering spectroscopy reveals a monotonic increase in both Sn and carbon incorporation. X-ray diffraction reveals tensile-strained films that are pseudomorphic with the substrate. Raman spectroscopy suggests substitutional C incorporation; both x-ray photoelectron spectroscopy and Raman suggest a lack of graphitic carbon or its other phases. For the lowest growth temperatures, scanning transmission electron microscopy reveals nanovoids that may account for the low Sn substitutional fraction in those layers. Conversely, the sample grown at high temperatures displayed abrupt interfaces, notably devoid of any voids, tin, or carbon-rich clusters. Finally, the surface roughness decreases with increasing growth temperature. These results show that atomic hydrogen provides a highly promising route to increase both Sn and C to achieve a strongly direct bandgap for optical gain and active silicon photonics.

Published under an exclusive license by AIP Publishing. https://doi.org/10.1063/5.0173429

I. INTRODUCTION

Direct integration of an efficient Group-IV laser with silicon remains an unachieved objective for unlocking the full potential of silicon photonics technology. Indirect bandgaps of Group-IV semiconductors limit the radiative recombination rates, leading to low quantum efficiency and demanding high threshold current. Interestingly, the small energy difference $(136\,\text{meV})^1$ between the direct (Γ -symmetry) and indirect (Γ -symmetry) conduction band valley in Ge can be overcome by tensile strain or alloying with tin

(Sn) and/or carbon (C), potentially paving a path to achieving efficient light emission. Electrically pumped Ge lasers on Si, with tensile strain from the thermal expansion mismatch, have been demonstrated at room temperature, but high threshold current densities (280 kA/cm²) preclude photonic applications.² Devices such as photodetectors, modulators, and light-emitting diodes (LEDs) based on GeSn-based binary alloy have been demonstrated, 3,4 but electrically injected GeSn lasers only operate at cryogenic temperatures, pulsed, and/or very high thresholds. 5 Another binary alloy, dilute $\text{Ge}_{1-y}\text{C}_y$ with $y \approx 0.01$ has been predicted to have a strong direct bandgap

⁶Department of Physics, University of Michigan, Ann Arbor, Michigan 48109, USA

a) Present address: Sandia National Laboratory, Sandia, New Mexico 87185, USA.

b) Author to whom correspondence should be addressed: mwistey@txstate.edu

with strong optical transitions.^{6,7} However, typical crystal growth techniques (arc-plasma) and carbon precursors (graphite cathode) have resulted in unwanted graphitic (sp²) or other carbon defects, partly because non-substitutional C is energetically favorable over the desired tetrahedrally bonded incorporation into the crystal.

The ternary alloy GeSnC is anticipated to offer superior growth benefits when compared to its binary counterparts, GeSn and GeC. Additionally, the Vienna Ab initio Simulation Package (VASP), based on density functional theory (DFT), found that the bandgap of GeSnC relies on its nearest-neighbor arrangement. In a 128-atom supercell, with 1 Sn and 1 C atom (0.78% each), the direct bandgap ranges from 0.486 to 0.401 eV, depending on Sn's position relative to carbon in the Ge lattice. 10 The indirect L valley remains mostly unchanged, remaining above 0.6 eV with the addition of C or Sn. These predictions suggest that GeSnC holds potential as a promising direct bandgap material for next-generation Si photonics lasers. Notably, our recent research demonstrated successful molecular beam epitaxy (MBE) growth of a high-quality GeSnC material, employing carbon tetrabromide (CBr₄) as the carbon precursor. 11 The material exhibits good crystallinity, and atomically flat surfaces without evidence of unwanted C phases, defects, or alternate Sn (B) phases. However, the assumption that Sn incorporation in the GeSnC samples mirrors the unity sticking coefficient observed in equivalent C-free GeSn samples was found invalid through subsequent Rutherford backscattering spectrometry (RBS) measurements.¹² RBS showed six times less (83%) Sn in GeSnC than the equivalent CBr₄-free GeSn sample grown under identical conditions. We also observed, in a separate study, 13 that as the CBr₄ pressure increases, the Sn atomic percentage concentration tends to decrease, and at a very high CBr₄/Sn ratio, the %Sn saturates at a minimum value close to the thermodynamic solubility limit. We attributed this phenomenon to the etching effect of bromine in GeSnC growth, forming volatile SnBr_x species.

The successful incorporation of both Sn and C in GeSnC growth is crucial for achieving the desired direct gap and efficient light emission. To enhance Sn and C incorporation, removing bromine from the growth surface becomes a key factor.

In this study, we investigated whether thermally cracked hydrogen atoms would assist in Sn incorporation in GeSnC growth by suppressing the etching of Sn by Br. The bond dissociation energy of H-Br is higher (365 kJ/mol) than Br-Sn (337 kJ/mol). Therefore, supplying atomic hydrogen to the surface during growth is expected to remove Br in the form of HBr, leaving Sn unaffected. Cheng et al. observed such removal of halogens by atomic hydrogen from Si (001) surfaces. 15 We systematically grew samples by introducing thermally cracked hydrogen to the growth process at temperatures suitable for alloy growth. Material properties were extensively characterized using atomic force microscopy (AFM), high-resolution x-ray diffraction (HRXRD), RBS, x-ray photoelectron spectroscopy (XPS), scanning transmission electron microscopy (STEM), and Raman spectroscopy. Understanding the effects of atomic hydrogen on growth would aid in further optimization of GeSnC epitaxy.

II. EXPERIMENTAL DETAILS

In this paper, we examined three sets of GeSnC samples grown by MBE, employing Ge and Sn solid source effusion cells, along with commercially available, high-purity CBr₄ as the carbon precursor. The first two sets were grown as in Ref. 11 using GaAs as a substrate, but the second added thermally cracked hydrogen (atomic H) to study its efficacy in bromine removal. The GaAs (001) substrates were unintentionally doped, quartered coupons extracted from 3-in. epi-ready, double-sided polished wafers. The third set of samples was grown on single-side polished, p-doped Ge (001) substrates. Ge and GaAs have virtually identical lattice constants, and the substrate was buried by a 155 ± 2 nm (verified by STEM) Ge buffer in all cases, so the choice of substrates is believed to have no effect apart from the possible differences in growth temperature (see the supplementary material). Even so, the results and analyses in the paper were organized without mixing samples grown on different types of substrates, thereby ensuring that the results remained unaltered by the substrate's nature. Band edge thermometry (k-Space Associates BandiT) and indium droplet melting were used to calibrate the substrate heater thermocouple. For consistency, this paper reports thermocouple temperatures (in °C and, hereafter, denoted TC) rather than an implied surface temperature (°C); comparative calibrations of surface temperature (°C) and thermocouple temperature (TC) can be found in the supplementary material.

A commercial atomic hydrogen source (Veeco Atom-H) was used to desorb native oxide during growth. A filament current of 8.5 A produced a nominal temperature of 2260 °C for ~11% cracking efficiency. The native oxide on the Ge and GaAs substrates was thermally removed at 320 and 375 TC, respectively, under a beam of thermally cracked hydrogen (atomic H). Reflection high-energy surface reconstruction. RHEED showed bright 2×4 or 4×2 patterns on GaAs substrates, or 2× reconstruction. strates, after 20 min of atomic H exposure, verifying an oxide-free surface. Although the accurate RHEED azimuthal/crystal direction was not recorded, the reconstruction pattern was based on the $^{\mbox{\scriptsize ω}}$ recurring pattern that appeared on a substrate's fixed rotation. RHEED images can be found in the supplementary material.

Prior to growing the GeSnC film, regardless of the substrate, a 155 ± 2 nm Ge buffer layer was grown at 400 TC. RHEED verified a uniform, flat surface with a 2×2 reconstruction pattern, typically indicating a smooth, Ge-terminated surface. A similar sample of Ge on GaAs at the same temperature showed a flat surface verified by AFM (RMS roughness 0.5 nm over $10 \times 10 \,\mu\text{m}$; see the supplementary material). Next, a GeSnC layer with a thickness of $215 \pm 2 \text{ nm}$ (verified by STEM) was grown at low temperatures (160-220 TC) to avoid Sn segregation. The beam equivalent pressures (BEPs) of Ge, Sn, and CBr_4 were held constant (Ge = 1.6×10^{-9} Torr, Sn = 6.7×10^{-9} Torr, $CBr_4 = 3 \times 10^{-7}$ Torr) throughout the growth. Atomic H was used during GeSnC deposition at a background pressure of 1×10^{-5} Torr, measured by an ion gauge. The residual gas analyzer (RGA) showed that H2 partial pressure was in the same order of magnitude as background pressure. Unless otherwise stated, a 10 nm Ge cap layer was deposited on the GeSnC layer to enable photoluminescence measurements, which will be presented elsewhere.

To study surface morphology, AFM was used in tapping mode under ambient conditions using Si probes with a nominal tip radius of 8 nm. The atomic percentages were obtained based on

RBS measurements. The random and channeled spectra were recorded to assess the crystallinity of the alloy. The measurements were conducted at the Michigan Ion Beam Laboratory (MIBL) using a 1.7 MV General Ionics tandem ion accelerator. The beam spot size was $1 \times 1 \text{ mm}^2$ with a maximum beam divergence of 0.05°. Backscattered particles were detected by a silicon surfacebarrier detector located at 170° with respect to the incident beam direction. 16,17 Samples were mounted on an automated five-axis goniometer to allow channeling measurements in the [001] axis. HRXRD measurements were performed using a Rigaku diffractometer with Cu K α 1 radiation ($\lambda = 1.540597 \text{ Å}$) and a Ge (220) monochromator. Rocking curves (RC), RSM, and 2θ-ω scans were performed to determine the crystal quality, strain, and substitutional incorporation of C in each film. XPS measurements were performed using a ThermoFisher Nexsa system using Al Kα (1486.6 eV) monochromatic x rays with an energy resolution of ≤0.5 eV. In situ Ar ion etching was used to remove surface contamination and partially etch the GeSnC layer. Sample charging was neutralized using an electron flood gun. Each spectrum used the C1s peak at 284.8 eV for charge correction. Unpolarized micro-Raman measurements were conducted using a Horiba LabRam with 632.8 nm excitation. The optical penetration depth at this wavelength is only ~30 nm in Ge; 18 hence, the light probes only the alloy (and 10 nm Ge cap where present) without appreciable scatter from the underlying layer. The laser spot was focused onto the surface using a 100x objective lens (NA 0.64) with power at the source kept at 10 mW to avoid local heating. To obtain an acceptable signal-to-noise, particularly for the carbon local vibrational mode (C-LVM), 15 identical acquisitions were obtained with an exposure time of 80 s followed by direct summing of the individual spectra. All the Raman modes observed in the alloy are identified based on previous reports. 11 In this report, we focus on the C-LVM range of the Raman spectra. STEM analysis to investigate crystal orientation, defects, and thickness of the grown epi-layers was done using a Thermo Fisher Talos 200i at an accelerating voltage of 200 kV. Samples were prepared by focused ion beam milling using a Ga⁺ ion beam with final polishing done at 5 kV followed by broad beam Ar+ ion milling done at 0.8 kV.

III. RESULTS AND DISCUSSION

A. Surface morphology

Figure 1 presents AFM images over an area of $10 \times 10 \,\mu\text{m}^2$ for GeSnC samples grown both with and without the presence of atomic hydrogen (H) at temperatures of 180 and 200 TC. These samples were grown without a Ge cap layer. The films grown without atomic hydrogen exhibited flat surfaces with root mean square (rms) roughness values below 0.4 nm. In contrast, the equivalent samples grown with atomic hydrogen displayed slightly higher rms roughness values of 1.7 and 1.2 nm, respectively.

We attribute the higher roughness observed in the GeSnC samples grown with atomic hydrogen to the interaction of hydrogen with carbon (C). Previous studies have demonstrated that active hydrogen helps to effectively suppress island growth in pure germanium (Ge) and $Ge_{1-x}Sn_{x}$ On the other hand, facets were found in $Ge_{1-v}C_v$ growth when using a hydrogenated carbon source.²¹ To demonstrate the interaction of atomic H and carbon, the equivalent Sn-free Ge_{1-v}C_v sample grown at 200 TC shows a comparable rms roughness of 1.4 nm, Fig. 1(e),²² which is consistent with the findings for the equivalent GeSnC sample grown at the same temperature, Fig. 1(d).

Therefore, the slightly elevated roughness observed in the GeSnC samples grown with atomic hydrogen may be attributed to an interaction between active hydrogen and carbon (C).

In situ RHEED was used to monitor growth and surface reconstruction in real time. A comparative analysis of the RHEED images obtained from the samples subjected to growth under the presence of atomic H and those grown without atomic H is E shown in Fig. 2. In all instances where samples were grown without $\frac{8}{8}$ atomic H, a discernible streak-like RHEED pattern was 8 observed, exhibiting a 2X reconstruction, in the temperature range of 160-220 TC (°C). This distinctive RHEED pattern showed a § smooth surface morphology.

Conversely, the samples subjected to growth with the presence of atomic H displayed a spotty RHEED pattern, suggesting a threedimensional (3D) growth at those temperatures, with an exception of the samples grown at 220 TC, which showed streaky RHEED.

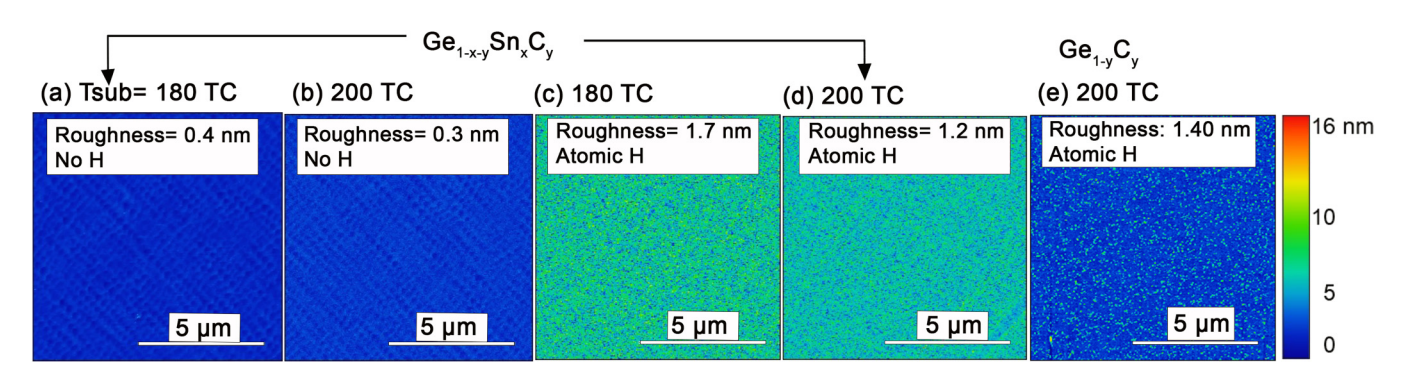


FIG. 1. AFM images $10 \times 10 \, \mu \text{m}^2$ for GeSnC samples grown on GaAs without atomic H [(a) and (b)] and with atomic H [(c) and (d)] at 180 and 200 TC, respectively. (e) AFM image of an equivalent $\text{Ge}_{1-y}\text{C}_y$ sample grown on GaAs with atomic H (after Ref. 22). The same color scale is used for all images. AFM images [(a) and (b)] are reproduced with permission from Appl. Phys. Lett. **121**, 122104 (2022). Copyright 2022 AIP Publishing LLC.

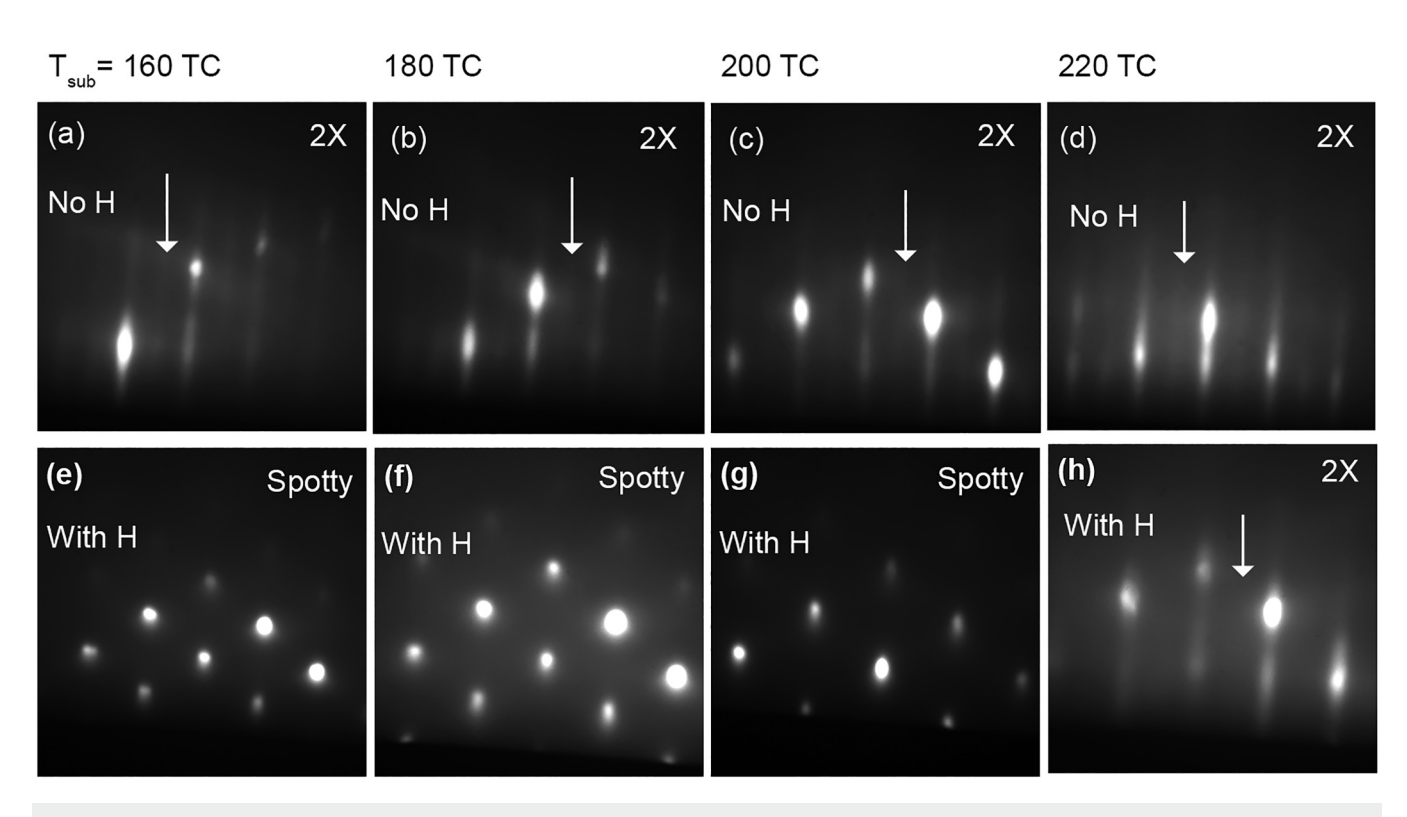


FIG. 2. RHEED images for GeSnC samples grown on GaAs with and without atomic H at different growth temperatures. RHEED images [(a)–(d)] are reproduced with permission from Appl. Phys. Lett. 121, 122104 (2022). Copyright 2022 AIP Publishing LLC.

AFM was consistent with the RHEED results, showing 1.7 and 1.2 nm roughness for samples grown at temperatures of 180 and 200 TC, and displayed a maximum feature height of 16 nm. As will be discussed below, for the layers grown in the temperature range (160–200 TC), post-growth STEM reveals the presence of voids.

B. Carbon defects and bonds

Density functional theory modeling using the Vienna Ab initio Package Simulation (VASP)^{23,24} showed that the bonding of C with a single Sn as the first nearest neighbor is \sim 0.30 eV more favorable than Sn as the second nearest neighbor.¹⁰ Carbon and tin partially compensate for each other's local distortion of both the nearby lattice and the band structure.

However, carbon may also precipitate in the alloy as "C–C" defects. Such precipitated C atoms were previously reported in GeSnC alloys at a binding energy of ~285 eV in XPS. ²⁵ In the present study, XPS was performed to investigate the chemical bonding state and test whether $\rm sp^2/sp^3$ carbon defects were detectable in the alloy. The XPS core energy spectra of Ge 3d, Sn 3d, and C 1s are shown in Figs. 3(a)–3(c) for the GeSnC sample grown with atomic H at 180 TC. The elemental Ge 3d core energy spectrum was deconvoluted with two Gaussian peaks corresponding to Ge 3d_{3/2} (29.7 eV) and Ge $\rm 3d_{5/2}$ (29.1 eV); see Fig. 3(a). Since this alloy is 97% Ge, no significant peak shift or features are present in

the Ge 3d XPS spectra. A similar sample grown without atomic H also showed the same peak position for Ge 3d.

The C 1s core energy spectrum was fitted with a single Gaussian function centered at 282.4 eV, indicating that the C1s peak represents both C-Sn and C-Ge bonds in the alloy or a combination of both. However, attempts to fit a peak at approximately 285 eV failed, showing that sp²/sp³ carbon defects were below the detection limits, shown in Fig. 3(b). An asymmetric least-squares smoothing function was used for baseline correction; the raw data with the fitted baseline can be found in the supplementary material.

Similarly, the Sn 3d core energy spectra were readily fitted with a single Gaussian peak centered at 484.7 eV, shown in Fig. 3(c). Therefore, the Sn 3d band may represent Sn–C or Sn–Ge bonds, or a combination of both with peaks too close to resolve. The corresponding GeSnC sample grown without atomic hydrogen also exhibited a Sn 3d peak at the same binding energy of 484.3 eV [Fig. 3(d)]. The lower Sn 3d peak intensity for the sample grown without atomic H is due to the decrease in Sn incorporation. Finally, the absence of a Br 3d peak (at 68.7 eV) suggests the absence of Br incorporation during MBE.

C. Substitutional carbon incorporation

Carbon can substitutionally incorporate in the desired, tetrahedrally bonded sites of the predominantly Ge lattice. Carbon may also form undesirable defects, inclusions, or an alternate carbon

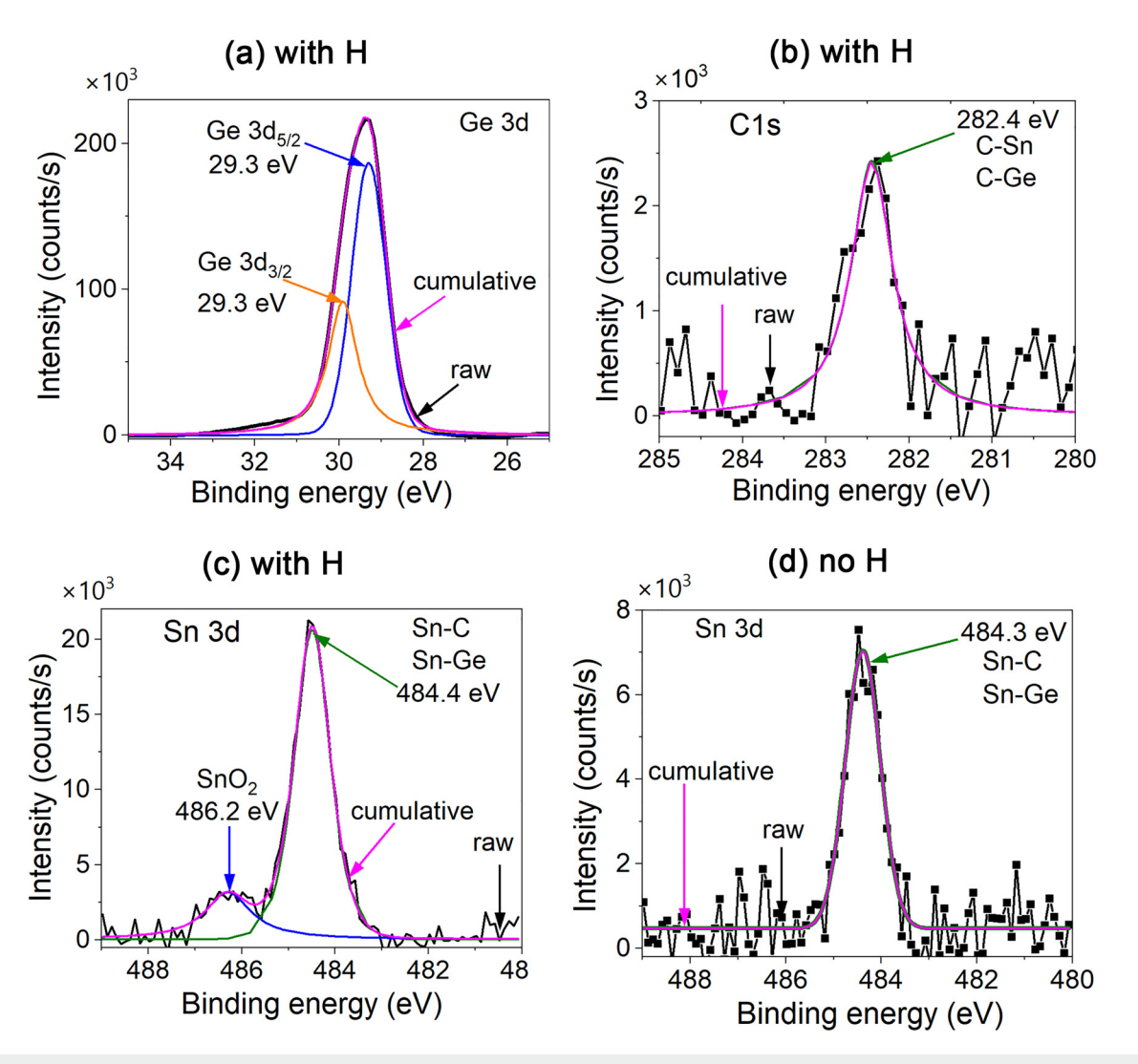


FIG. 3. XPS core energy spectra of Ge 3d, C1s, and Sn 3d for the GeSnC sample grown on the GaAs substrate with (a)–(c) or without (d) atomic H. The growth temperature was 180 TC.

phase, such as sp^2/sp^3 carbon, as reported in several $Ge_{1-y}C_y$ films.⁸ Raman spectroscopy was used to verify the substitutional incorporation of carbon and tested for the presence of alternate sp^2/sp^3 carbon phases within the GeSnC alloy. The use of a 632.8 nm wavelength laser provided a shallow penetration depth of approximately 30 nm in Ge and GeSnC, for an additional method to complement XPS for the detection of sp^2/sp^3 carbon.

Figure 4(a) shows the Raman spectra of GeSnC samples grown with atomic H and a Ge wafer as the control. Raman modes in GeSnC alloys in the $110-600 \text{ cm}^{-1}$ range were identified, including the $O(\Gamma)$ -symmetry first-order and multiple second-order (SO_{Ge}) scattering, as previously observed in bulk Ge. ²⁶ Intensities

were normalized to the first-order (Ge–Ge) and second-order (SO_{Ge}) scattering peaks located at $\sim\!\!300$ and $\sim\!\!571\,\mathrm{cm}^{-1}$, respectively. The first-order Raman-allowed Ge–Ge mode for the Ge wafer was observed at $300.7\,\mathrm{cm}^{-1}$, with a full width at half maximum (FWHM) of $2.5\,\mathrm{cm}^{-1}$. The GeSnC alloys similarly showed a narrow Ge–Ge band with a linewidth of less than $4\,\mathrm{cm}^{-1}$, confirming good crystal quality without large numbers of defects. It is worth noting that the Ge–Ge modes in all GeSnC samples shifted to lower wave numbers (redshift) than the Ge wafer,

$$\Delta \omega_{\text{Ge-Ge}} = \omega_{\text{Ge-Ge(GeSnC film)}} - \omega_{\text{Ge(Ge wafer)}} < 0. \eqno(1)$$

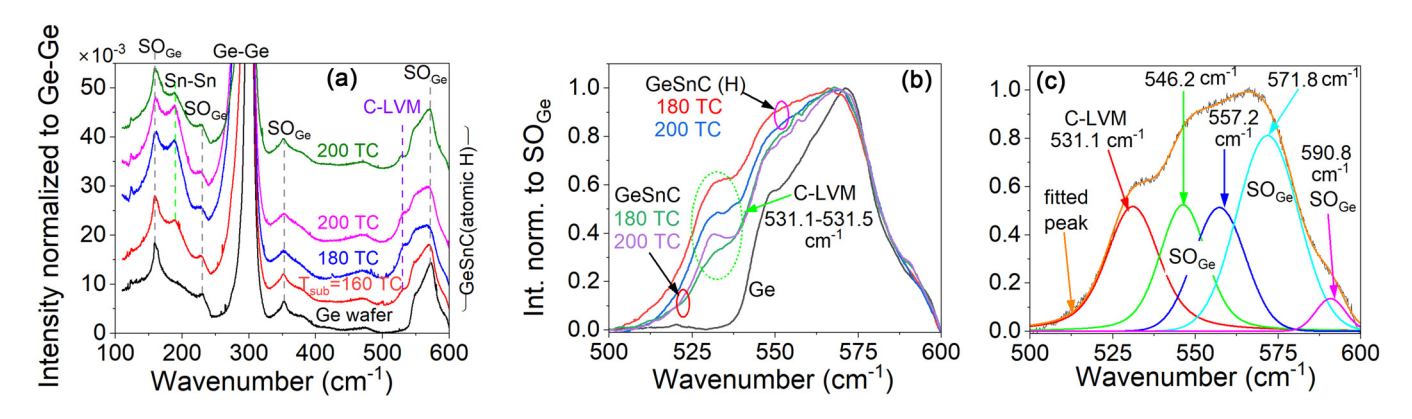


FIG. 4. Raman spectra for GeSnC samples grown on GaAs with atomic H at different temperatures, (a) Showing all vibrational modes, (b) C-LVM for GeSnC samples grown with and without atomic H at 180 and 200 TC. (c) Example fitting of the 180 TC + H sample to distinguish the C-LVM mode from SO_{Ge} peaks.

The maximum red shifting $(\Delta\omega_{\text{Ge-Ge}} = -1.05 \text{ cm}^{-1})$ occurred for the sample grown with atomic hydrogen at a growth temperature of 180 TC. Interestingly, for GeSnC grown with atomic H, a more pronounced shift is apparent, implying a greater extent of alloy-induced strain due to enhanced Sn in the alloy.

The second-order scatterings for Ge (SO_{Ge}) were present at 160, 230, 350, 546, 556, 571, and 592 cm⁻¹, as previously reported by other groups. Along with Ge-Ge and SOGe, another band near 185 cm⁻¹ was observed, attributed to Sn-Sn bonds.²

Figure 4(a) shows weak features in the range where the carbon local vibrational mode (C-LVM) has been previously reported near 531 cm⁻¹.28 As shown in the more detailed view in Fig. 4(b), the

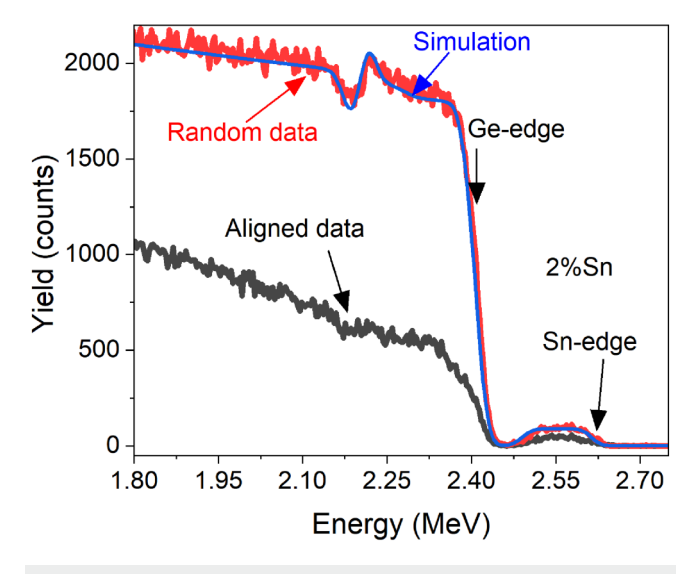


FIG. 5. Channeling-RBS spectra as a function of backscattered energy, for the GeSnC sample grown on GaAs with atomic H at 160 TC. The random and [001] channeling data are shown as red and black solid lines. SIMNRA simulation (solid blue line) indicates 2% Sn.

GeSnC alloys grown with and without H clearly exhibit the C-LVM band. Detailed fitting was carried out in the C-LVM range of each Raman spectrum, as shown in Fig. 4(c) for the GeSnC alloy grown at 180 TC with H. Line shapes were modeled using the Voigt function. In all cases, the SO_{Ge} bands were found to remain consistent in position and linewidth, and the C-LVM energy remained in the 531.1-531.5 cm⁻¹ range. The presence of the C-LVM band in all GeSnC samples, regardless of whether they were grown with or without atomic hydrogen, serves as a direct confirmation of the substitutional incorporation of carbon in the alloy.

Raman spectra over 1200–1600 cm⁻¹ were also measured to test for the presence of disordered carbon phases, 29 particularly near 1350 and 1540–1600 cm⁻¹. We observed no Raman features 4 in this range and constant 1.1. in this range and concluded that these carbon phases are not $\frac{3}{8}$ present in abundance using the growth techniques used here. The spectra for samples grown with atomic H are shown in the supplementary material.

D. Atomic percentages of TIN

To determine the absolute Sn content in each GeSnC film, RBS measurements were carried out using α particles and analyzed using the Simulation of Nuclear Reaction Analysis (SIMNRA) code.³⁰ Both random and [001] channeling-RBS spectra for the sample grown at 160 TC are shown in Fig. 5. A distinct peak near 2.55 MeV corresponds to the presence of Sn in the layer, and analysis using SIMNRA yielded a Sn composition of 2.0%.

Figure 6 shows a comparison of the atomic percentages of Sn measured by RBS in GeSnC samples grown with and without atomic H. The atomic percentages of Sn measured by HR-XRD from C-free GeSn samples are added as a control. The GeSn sample grown at a temperature of 160 TC exhibited Sn content of 3.7% as determined by RBS and 3.8% as determined by HR-XRD, which demonstrated strong agreement between the RBS and XRD results, further corroborating the consistency and accuracy of the obtained Sn content by HR-XRD in the GeSn alloy.

The Sn content for the GeSnC sample grown at 160 TC without atomic hydrogen measured as 0.6%. A direct comparison of this result with the equivalent GeSn sample reveals that the

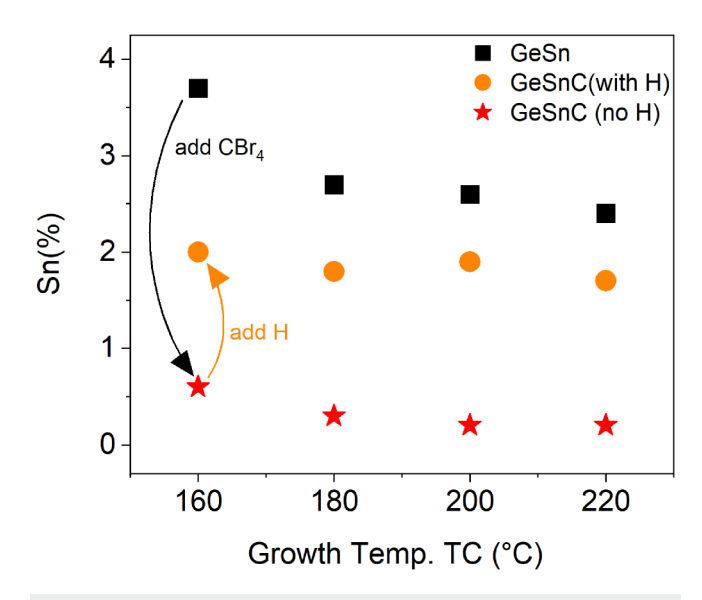


FIG. 6. Atomic percentages of Sn in GeSnC samples grown with and without atomic H at various temperatures on GaAs. The atomic percentages of Sn from equivalent, CBr_4 -free GeSn samples are also included.

GeSnC sample exhibits a remarkably lower Sn content, approximately 6x less, compared with the carbon-free GeSn counterpart.

However, the equivalent GeSnC sample grown with atomic H at 160 TC exhibited a Sn content of 2% measured by RBS, 3.3x times more Sn than the sample grown without atomic H. Thus, atomic H recovered approximately 38% of Sn that would otherwise be lost due to bromine etching. A similar trend was observed for the GeSnC samples grown at higher temperatures. Without H, RBS measurements revealed Sn contents of 0.4%, 0.2%, and 0.2% for the samples grown at 180, 200, and 220 TC, respectively. This is 9x, 13x, and 12x less Sn than the equivalent GeSn samples. In contrast, the equivalent samples grown with atomic H exhibited Sn contents of 1.8%, 1.9%, and 1.7% for the respective temperatures, which is a 6x, 9.5x, and 8.5x respective increase in Sn compared with the equivalent samples grown without atomic H. A maximum of 71% Sn is recovered for the sample grown at 200 TC with atomic H. The results are summarized in Table I.

The increase in the Sn content observed in the GeSnC samples is attributed to the elimination of bromine (Br) from the

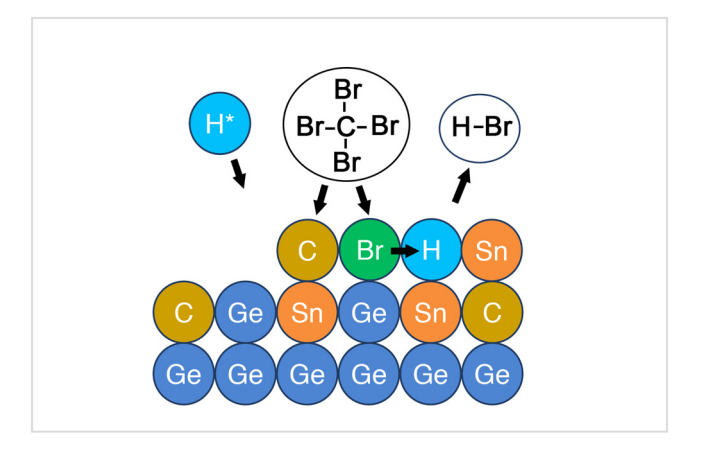


FIG. 7. Proposed mechanism for the removal of Br during GeSnC growth with atomic H

growth surface by atomic hydrogen (H) before it can etch Sn. During the growth process, CBr₄ delivers carbon (C) and Br to the growth surface. In the absence of atomic H, Br readily bonds with Sn, leading to the etching of Sn from the alloy. However, in the presence of atomic H, bromine atoms exhibit a preference for bonding with hydrogen rather than with Sn. This preference for H-Br bonding arises due to its higher bond dissociation energy (365 kJ/mol) compared with the Br-Sn bond (337 kJ/mol). Since Since gas-phase reactions are negligible in the high vacuum system (ranging from 10^{-5} to 10^{-9} Torr), only surface reactions are \aleph expected to govern the reaction of bromine by atomic H. The strong H-Br bond forms volatile HBr, which rapidly evaporates 👸 from the growth surface. During growth, the RGA detected distinct "S peaks of HBr at 80 and 82 amu. However, the RGA was not directly in the line of sight of the wafer, and scans to higher masses (SnBr_x) are currently unavailable. The growth mechanism is shown in Fig. 7.

E. Crystal quality and substitutional incorporation

In ion channeling measurements, the yield ratio χ_{\min} , which compares the backscattered yield between the channeled and random directions, serves as a quantitative measure of crystal quality and substitutional incorporation. In a highly crystalline Ge

TABLE I. RBS channeling data (Sn composition, χ_{min} , S) for GeSnC/GaAs grown with and without atomic H. S is substitutional fraction of Sn in the alloy.

Temp (TC)	GeSn %Sn (XRD)	GeSnC without atomic H				GeSnC with atomic H				
		%Sn	$\chi_{\rm min}$ for Ge	$\chi_{\rm min}$ for Sn	S (%)	%Sn	$\chi_{\rm min}$ for Ge	$\chi_{\rm min}$ for Sn	S (%)	Sn restored (%)
160	3.7	0.6	0.13	0.19	87	2.0	0.27	0.45	59	38
180	2.7	0.3	0.09	0.22	84	1.8	0.17	0.42	62	56
200	2.6	0.2	0.11	0.21	84	1.9	0.14	0.39	65	71
220	2.4	0.2	0.10	0.21	85	1.7	0.07	0.13	92	68

sample, the backscattered yield from the axially aligned ion beam is a small percentage of the random yield because the ions are steered by atomic rows into the crystal channel where they have a low probability of a close encounter collision. When solute atoms, such as Sn, are displaced into the crystal channel, the backscattered yield increases. For the sample grown at 160 TC using atomic H, χ_{min} values of 0.27 and 0.45 were obtained for Ge and Sn, slightly higher than those for Ge, and much higher than typical MBE-grown GeSn $(\chi_{min} \sim 0.1)$, indicating reduced crystallinity for low-temperature growth of GeSnC. As the growth temperature is increased, χ_{min} decreases (Table I) were observed, suggesting enhanced crystallinity.

RBS is also used to calculate the percentage of Sn atoms located on substitutional lattice sites (S) using Eq. (2) and χ_o , the minimum yield of a Ge reference crystal.

$$S = \frac{1 - \chi_{\text{minfor Sn}}}{1 - \chi_o} \times 100\%. \tag{2}$$

Figure 8 shows the fraction of substitutional Sn for the GeSnC samples grown with and without atomic H from 160 to 220 TC, along with the GeSn sample grown at 160 TC. Table I includes a list of the $\chi_{\rm min}$ values for Ge and Sn and S for Sn. For the samples grown without atomic H, the fraction of substitutional Sn is independent of growth temperature, with all values in the range of 84%-87%. In contrast, for the samples grown with atomic H, as the growth temperature is increased, χ_{\min} and S improved, indicating a better crystal quality and a higher fraction of substitutional Sn. For the atomic H-grown samples, the fraction of substitutional Sn increases from 59% to 92% with increasing growth temperature.

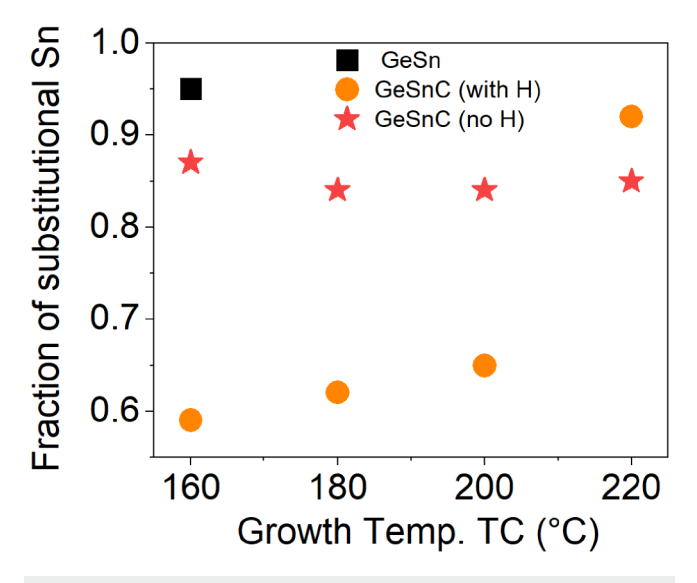


FIG. 8. Fraction of substitutional Sn determined from a comparison of random and channeling-RBS data for GeSnC/GaAs grown at various temperatures, with and without atomic H, in comparison with that of GeSn/GaAs grown at 160 TC.

It is worth noting that the fraction of Sn that incorporates substitutionally into the Ge lattice is lower in the samples grown with atomic H compared to the equivalent samples grown without atomic H, with the exception of the samples grown at 220 TC. At a growth temperature of 220 TC, the majority of Sn atoms occupy Ge sites, with minimal distortion.

To elucidate the variability in Sn substitutional atoms within the grown samples, STEM analysis was conducted on the GeSnC samples grown with atomic H at 160 and 220 TC. Annular dark field STEM (ADF-STEM) images most clearly differentiated the layers and, for both samples, showed that all interfaces were distinct, abrupt, and flat (GaAs/Ge, Ge/GeSnC, and GeSnC/Ge), without any visible interfacial dislocations. However, the Ge cap layers exhibited island formation, presumably due to limited Ge/GeSnC wetting. Additional high-angle annular dark field (HAADF) images were taken from both samples to identify regions of composition variation and neither showed evidence of Sn-rich or C-rich regions. For the sample grown at 160 TC, many circular defects in the GeSnC layers are apparent, beginning ~15 nm from the underlying Ge buffer, as shown in Fig. 9(a). The defect diameters ranged from roughly 10 to 30 nm. Convergent beam electron diffraction (CBED) confirmed that the circular regions were significantly thinner than the surrounding material. Energy dispersive spectroscopy (not shown) measurements showed increased Sn content surrounding the regions, suggesting that they are hollow nanovoids lined on the outside with Sn, or perhaps, Sn-rich GeSn. The Sn lining is presumably non-coherent with the Ge lattice and is consistent with the elevated $\chi_{\rm min}$ and the reduced fraction of substitutional Sn. We speculate that these defects could be the result of vacancies formed at low temperature, agglomerating into nanovoids during the subsequent high temperature Ge cap growth. However, 8 detailed studies of the origins and compositions of these defects are beyond the scope of the present paper.

On the other hand, for the GeSnC samples grown at high temperatures (220 TC), the circular defects, Sn-rich regions, and carbon clusters are not apparent [Figs. 9(b) and 9(d)].

F. Atomic percentage of carbon

High-resolution x-ray diffraction (HR-XRD) was used to determine the film's crystal quality, relaxation, and atomic percentages of carbon in the GeSnC alloy. The GeSnC ternary alloy is subjected to pseudomorphic strain induced by the GaAs substrate, which has been verified through reciprocal space mapping (RSM), as explained below. With the in-plane lattice constant (a_{\parallel}) known, the perpendicular lattice constant (a1) becomes the sole independent strain parameter. This, however, poses a challenge in the simultaneous determination of both x and y in the GeSnC alloy using HR-XRD, since each of them impacts the lattice constant.

To address this issue, the atomic percentage of Sn is taken from the RBS measurement, as previously described, and considered a fixed parameter in XRD simulation. This enables the calculation of the atomic percentage of carbon in the GeSnC ternary alloy.

A comparison of the HR-XRD 2θ-ω scans for the GeSnC samples grown on GaAs, with and without atomic hydrogen, is shown in Fig. 10(a). The growth temperatures are 160, 180, 200, and 220 TC. The diffraction peaks observed at 66.04° and 65.94°

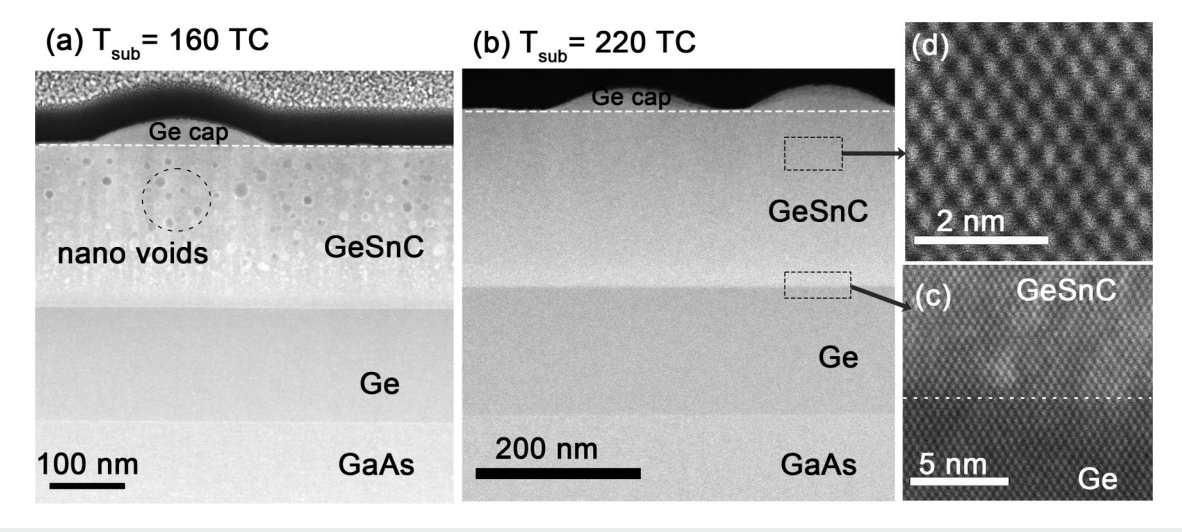


FIG. 9. Cross-sectional ADF-STEM images of the GeSnC samples grown on GaAs at (a) 160 and (b) 220 TC. (c) Magnified ADF-STEM image of the Ge/GeSnC interface, (d) Magnified HAADF image of the GeSnC layer.

correspond to the GaAs (004) substrate and Ge buffer layers, respectively. The well-defined peak at a higher diffraction angle represents the GeSnC layer. Pendellösung fringes are more pronounced in the samples grown without atomic H, indicating the presence of abrupt and flat interfaces. However, these fringes are less prominent in samples grown with atomic H. As mentioned earlier, the interaction of atomic H with C could potentially result in a slightly rougher surface, which may explain the less abrupt and flat interfaces observed in the atomic H-grown samples. Nonetheless, both sets of samples exhibit good crystal quality, with rocking curve (RC) analysis yielding the highest full width at half maximum (FWHM) values of 66 and 55 arc sec for the samples grown with and without atomic H, respectively.

RSM was conducted for all samples around the asymmetric (115) reflection to assess the extent of relaxation. Figure 10(b) shows the RSM scan specifically for the sample grown at 160 TC, which exhibits the highest percentages of Sn (2%) and C (1.5%) among the four samples. The peaks corresponding to the GaAs substrate, Ge buffer layer, and GeSnC film all have the same Q_x position, indicating a matched in-plane lattice spacing with the substrate without any relaxation. For the GeSnC film grown at a substrate temperature of 160 TC, the out-of-plane lattice constant a₁ is determined to be 5.6329 Å.

The atomic percentages of carbon (C) from HRXRD are plotted in Fig. 11. For the samples grown with atomic H, the substitutional carbon percentages are measured as 1.5%, 1.4%, 1.4%, and 1.0% at 160, 180, 200, and 220 TC, respectively. The results are compared with the samples grown without atomic H, indicating that all samples grown with atomic H have higher substitutional carbon. For example, the sample grown at 160 TC measured 1.25x higher substitutional carbon than the equivalent sample grown without atomic H. Similarly, the other samples grown with higher temperatures show 1.16x, 1.4x, and 1.25x higher substitutional carbon.

In a separate study, we observed that Sn facilitates the incorporation of carbon, largely due to a partial cancellation of distortion that highly electronegative C atoms cause in the Ge host lattice, even when fully substitutional.³² Therefore, the higher carbon incorporation could be a side effect of the increase in Sn content in atomic H-grown samples. Additionally, the equivalent Sn-free GeC still grown with atomic H exhibited higher substitutional carbon compared to the sample grown without atomic H.²² Therefore, the § increase in substitutional carbon observed in atomic H-grown GeSnC is attributed to a combined effect of Sn and atomic H.

The larger 2θ angles indicate more tensile strain for all GeSnC $^{\mathfrak{S}}$ samples grown without atomic hydrogen than those grown with atomic H. In the case of atomic H-grown samples, the 2θ positions are shifted toward lower diffraction angles, as indicated by the red arrows in Fig. 10(a). Although H increases both %Sn and %C, the increase is higher for %Sn, shifting the alloy slightly toward a more compressive strain.

On the other hand, the concentrations of carbon (C) and Sn decrease at higher growth temperature (220 TC) for the atomic H-grown GeSnC samples, as indicated by the dashed blue line in Fig. 9(a). A similar decrease in %C and %Sn with growth temperature was also observed for the samples grown without atomic H.¹ This is consistent with the earlier findings that Sn reduces the energy cost of C incorporation, implying less Sn would also incorporate less C.

The out-of-plane (ε_{\perp}) and in-plane strain $(\varepsilon_{\parallel})$ were calculated using the same technique as described in Ref. 11. The results reveal the presence of residual in-plane tensile strain $(\varepsilon_{\parallel})$ in both types of GeSnC samples, with and without atomic H. However, the atomic H-grown samples exhibit lower in-plane tensile strain than those grown without atomic H. Substitutional Sn produces the opposite strain to C in Ge, and due to higher percentages of Sn, the atomic H-grown samples demonstrate lower in-plane tensile strain. The results are summarized in the supplementary material.

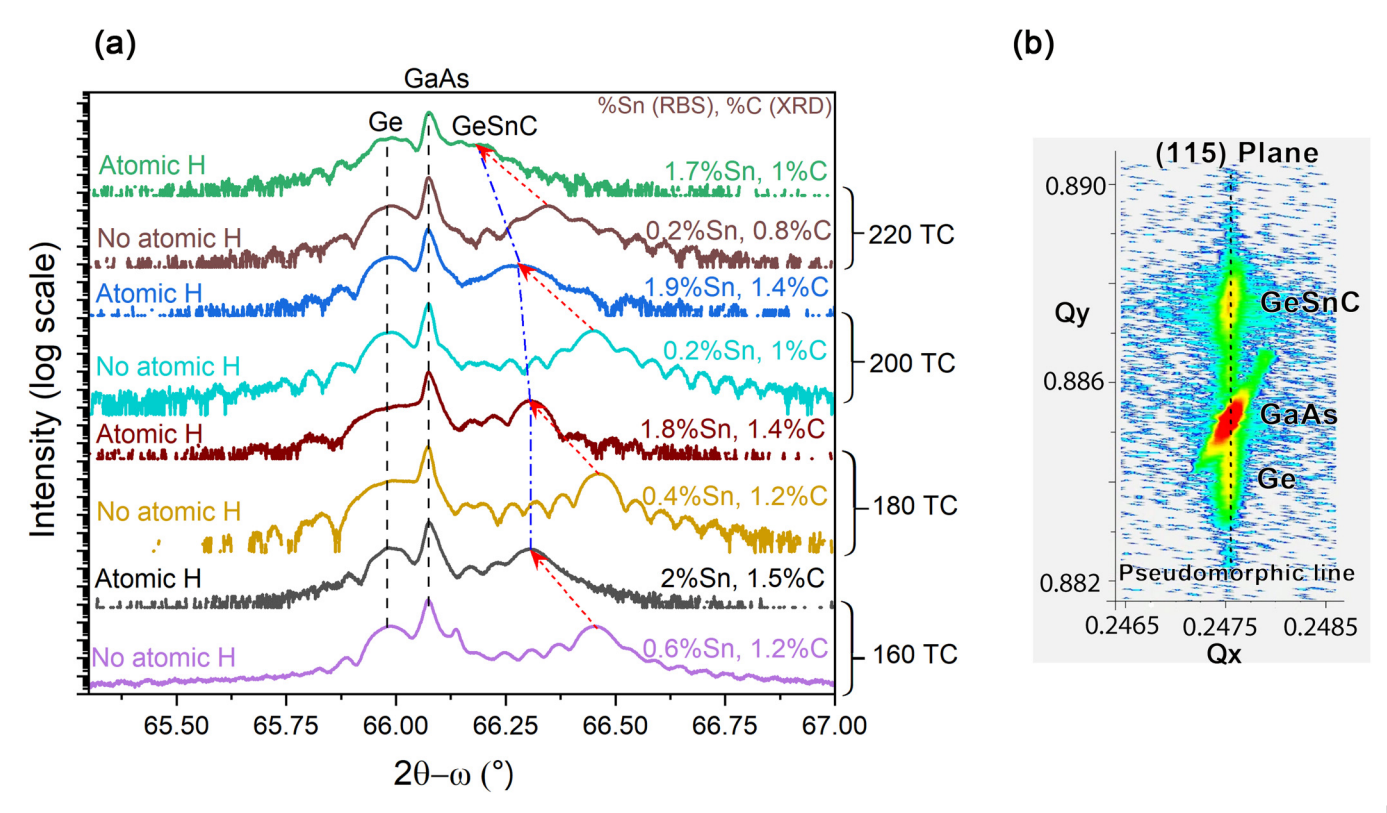


FIG. 10. (a) HR-XRD 2θ-ω scans for GeSnC samples grown on GaAs, with and without atomic H at different temperatures, (b) RSM scan for the GeSnC sample grown with atomic H at 160 TC.

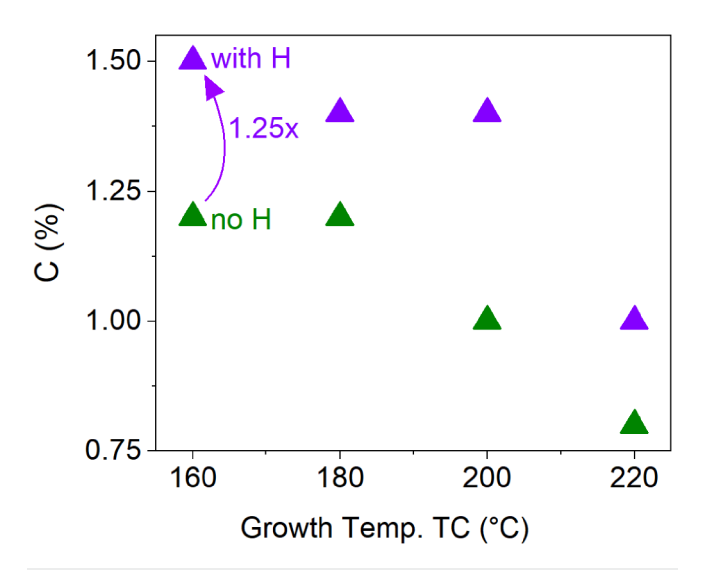


FIG. 11. %C from XRD fit for GeSnC grown on GaAs with and without atomic H at different temperatures, using %Sn from RBS.

G. I of H in bromine removal

We now use the samples grown on Ge to consider the role of atomic hydrogen pressure in removing bromine. During the growth experiment, the Sn beam flux was constant at $1.3\times 10^{-8},$ while the atomic hydrogen pressure varied within the range of $2\times 10^{-6}-10\times 10^{-6}$ Torr. Specifically, the first sample was grown at an atomic hydrogen pressure of 2×10^{-6} Torr, while the second sample was grown with a 5x higher atomic hydrogen pressure of 10×10^{-6} Torr.

XPS calibrated from RBS was performed on these samples to determine the atomic percentage of Sn. The sample grown with higher atomic H flux showed Sn = $2.0 \pm 0.1\%$, compared with $0.8 \pm 0.1\%$ with lower atomic H: a 2.5x increase in Sn from a 5x increase in H.

Figure 12 plots the above results for %Sn with an additional equivalent sample that was grown without atomic H. XPS measured 0.3 ± 0.1 %Sn for the sample grown without atomic H. It is evident from the plot that by increasing atomic H pressure, %Sn increases linearly, even if the Sn beam equivalent pressure remains constant, which demonstrates that Sn incorporation could be increased by increasing the atomic hydrogen pressure. This finding further supports our hypothesis that the formation of Sn–Br bonds can be controlled by the presence of atomic hydrogen on the

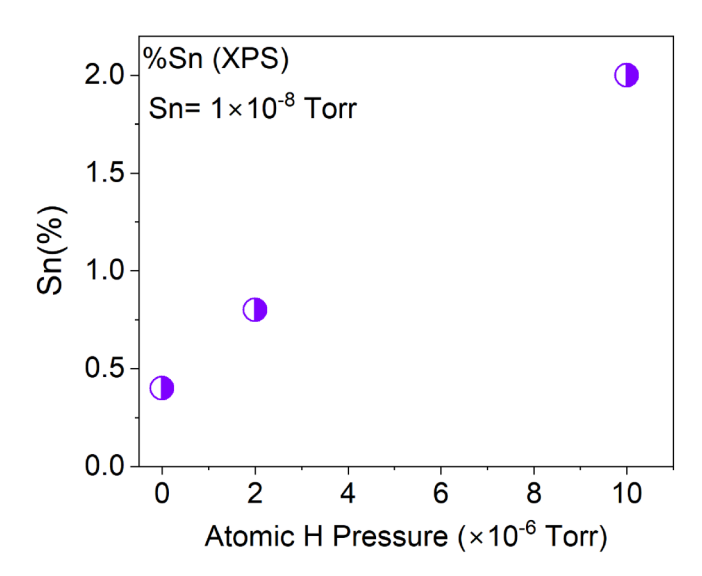


FIG. 12. %Sn measured by XPS for GeSnC samples grown on Ge by varying atomic H flux.

growth surface, and its effectiveness is enhanced by increasing the number of active hydrogen atoms.

XRD was utilized to determine the substitutional carbon content based on Sn measured by XPS. XRD analysis revealed a substitutional carbon content of 1.8% for the sample grown with a lower atomic H pressure and 1.9% for the sample that was grown with a higher atomic H pressure.

IV. SUMMARY

In summary, we found that the use of CBr_4 as a carbon precursor for GeSnC alloys significantly decreases the Sn content, but adding thermally cracked, atomic H restores most of Sn. We believe atomic H removes Br from the surface before it can attack Sn.

Furthermore, AFM showed atomically flat surfaces with comparable RMS roughness <1.7 nm for films grown with and without atomic H. RHEED revealed a temperature dependence in surface reconstruction. At lower temperatures, a three-dimensional (3D) growth pattern was observed, whereas higher temperatures promoted a smoother growth morphology.

Likewise, HR-XRD analysis revealed a comparable crystal quality between the films grown with atomic hydrogen and those grown without it. However, a subtle distinction was observed in atomic hydrogen-grown films, where the interface appears to be slightly less abrupt compared to the films grown without atomic hydrogen.

Raman spectroscopy confirmed the substitutional incorporation of carbon within the lattice, and Raman and XPS showed no detectable sp²/sp³ carbon or bromine in the alloy. These collective findings strongly suggest that the carbon incorporation process occurred exclusively in a substitutional manner, ruling out any unwanted nanoclusters or carbon defects.

Specifically, channeling-RBS data reveal that MBE of GeSnC in the presence of atomic hydrogen enhances Sn incorporation.

Notably, the Sn percentage increased by up to 9.5x in atomic hydrogen-grown samples. Further increasing the H flux by 5x increased %Sn by 2.5x. Channeling RBS also showed that the samples grown with atomic H have a lower fraction of substitutional Sn compared to those without, except the sample grown at 220 TC.

STEM showed nanovoids in the sample grown at a low temperature (160 TC), potentially contributing to the decreased Sn fraction in the alloy. Conversely, the samples grown at high temperatures exhibited a lack of defects, with distinct and well-defined interfaces.

Based on these comprehensive results, we conclude that the addition of atomic hydrogen is an effective strategy to increase the atomic percentage of tin (Sn) in GeSnC growth when CBr4 is used as the carbon source. Atomic hydrogen reacts with bromine immediately on the growth surface, forming highly preferable H-Br bonds that subsequently evaporate as HBr, preventing the etching of Sn as volatile SnBrx. Although further studies are required to fully understand the growth mechanism, it is evident that atomic hydrogen plays a crucial role in restoring approximately 38%-71% of Sn previously lost due to bromine etching in situ. Additionally, we observed a significant, simultaneous increase in substitutional carbon content in the samples, which can be attributed to the reduced local strain around the Ge lattice for increased Sn. Collectively, these findings highlight the efficacy of atomic H in enhancing Sn incorporation and optimizing the growth of GeSnC films using CBr₄ as the carbon precursor.

SUPPLEMENTARY MATERIAL

See the supplementary material for native oxide desorption using atomic hydrogen, Ge buffer growth, substrate temperature calibration using KSA BandiT, Raman measurement for sp²/sp³ carbon defects, XPS data with fitted baseline, and metrology results (atomic percentage of carbon, FWHM, and calculated strain) using x-ray diffraction.

ACKNOWLEDGMENTS

The authors gratefully acknowledge support from the National Science Foundation under Grant Nos. DMR-1508646, DMR-1810280, CBET-1438608, and PREM DMR-2122041 and The Center for Dynamics and Control of Materials (No. DMR-1720595) with additional support from the University of Texas at Austin. This work was also partially supported by the Coordenação de Aperfeiçoamento de Pessoal de Nível Superior—Brasil (CAPES)—Finance Code 001.

AUTHOR DECLARATIONS

Conflict of Interest

The authors have no conflicts to disclose.

Author Contributions

Tuhin Dey: Conceptualization (equal); Formal analysis (lead); Investigation (equal); Methodology (lead); Resources (lead); Validation (equal); Writing – original draft (lead); Writing –

review & editing (equal). Augustus W. Arbogast: Resources (equal); Writing - review & editing (supporting). Qian Meng: Resources (supporting); Writing - review & editing (supporting). Md. Shamim Reza: Resources (supporting); Writing – review & editing (supporting). Aaron J. Muhowski: Investigation (supporting). Joshua J. P. Cooper: Formal analysis (supporting); Investigation (equal); Resources (equal); Writing - review & editing (equal). Erdem Ozdemir: Resources (supporting). Fabian U. Naab: Resources (supporting). Thales Borrely: Formal analysis (supporting); Investigation (supporting); Resources (supporting); Writing - review & editing (equal). Jonathan Anderson: Formal analysis (supporting); Investigation (supporting). S. Goldman: Formal analysis (supporting); Funding acquisition (supporting); Investigation (equal); Supervision (equal); Validation (supporting); Writing - review & editing (equal). Daniel Wasserman: Funding acquisition (supporting); Supervision (supporting). Seth R. Bank: Funding acquisition (supporting); Investigation (supporting); Supervision (supporting); Writing review & editing (supporting). Mark W. Holtz: Formal analysis (supporting); Investigation (equal); Methodology (supporting); Writing - review & editing (equal). Edwin L. Piner: Investigation (supporting); Validation (supporting); Writing - review & editing (supporting). Mark A. Wistey: Conceptualization (lead); Formal analysis (equal); Funding acquisition (lead); Investigation (equal); Methodology (equal); Project administration (lead); Supervision (lead); Validation (equal); Writing – review & editing (lead).

DATA AVAILABILITY

The data that support the findings of this study are available from the corresponding author upon reasonable request.

REFERENCES

- ¹O. M. Landolt-Bornstein, *Physics of Group IV Elements and III–V Compounds:* Numerical Data and Functional Relationships in Science and Technology (Springer, Berlin, 1982).
- ²E. R. Camacho-Aguilera, Y. Cai, N. Patel, J. T. Bessette, M. Romagnoli, L. C. Kimerling, and J. Michel, Opt. Express 20(10), 11316 (2012).
- ³M. Oehme, J. Werner, M. Gollhofer, M. Schmid, M. Kaschel, E. Kasper, and J. Schulze, IEEE Photonics Technol. Lett. **23**(23), 1751 (2011).
- ⁴M. Oehme, K. Kostecki, T. Arguirov, G. Mussler, K. Ye, M. Gollhofer, M. Schmid, M. Kaschel, R. A. Körner, M. Kittler, D. Buca, E. Kasper, and J. Schulze, IEEE Photonics Technol. Lett. **26**(2), 187 (2014).
- ⁵Y. Zhou, S. Ojo, C.-W. Wu, Y. Miao, H. Tran, J. M. Grant, G. Abernathy, S. Amoah, J. Bass, G. Salamo, W. Du, G.-E. Chang, J. Liu, J. Margetis, J. Tolle, Y.-H. Zhang, G. Sun, R. A. Soref, B. Li, and S.-Q. Yu, Photonics Res. 10(1), 222 (2022)
- ⁶C. A. Stephenson, W. A. O'Brien, M. W. Penninger, W. F. Schneider, M. Gillett-Kunnath, J. Zajicek, K. M. Yu, R. Kudrawiec, R. A. Stillwell, and M. A. Wistey, J. Appl. Phys. **120**(5), 053102 (2016).

- ⁷I. A. Gulyas, C. A. Stephenson, Q. Meng, S. R. Bank, and M. A. Wistey, J. Appl. Phys. **129**(5), 055701 (2021).
- ⁸M. Okinaka, Y. Hamana, T. Tokuda, J. Ohta, and M. Nunoshita, J. Cryst. Growth 249(1), 78 (2003).
- ⁹J. D'Arcy-Gall, D. Gall, I. Petrov, P. Desjardins, and J. E. Greene, J. Appl. Phys. 90(8), 3910 (2001).
- ¹⁰Q. Meng, S. R. Bank, and M. A. Wistey, "Undoing band anticrossing in highly mismatched alloys by atom arrangement," J. Appl. Phys. (submitted).
- ¹¹T. Dey, M. S. Reza, A. Arbogast, M. W. Holtz, R. Droopad, S. R. Bank, and M. A. Wistey, Appl. Phys. Lett. **121**(12), 122104 (2022).
- ¹²T. Borrely, J. Cooper, T. Dey, A. W. Arbogast, F. Naab, M. A. Wistey, and R. Goldman, "Mechanisms for co-incorporation of Sn and C in GeSnC alloys" paper presented at the Electronic Materials Conference (EMC), Santa Barbara, CA (2023) (unpublished).
- ¹³T. Dey, A. W. Arbogast, J. J. P. Cooper, T. Borrely, R. S. Goldman, M. W. Holtz, M. A. Wistey, "Influences of carbon tetrabromide and tin flux on GeCSn epitaxy", (unpublished).
- 14B. deB. Daewent, Bond Dissociation Energies in Simple Molecules (NSRDS, 1970)
- ¹⁵C. C. Cheng, S. R. Lucas, H. Gutleben, W. J. Choyke, and J. T. Yates, Jr., J. Am. Chem. Soc. 114(4), 1249 (1992).
- ¹⁶T. Jen, G. Vardar, Y. Q. Wang, and R. S. Goldman, Appl. Phys. Lett. **107**(22), 221904 (2015).
- ¹⁷J. Occena, T. Jen, E. E. Rizzi, T. M. Johnson, J. Horwath, Y. Q. Wang, and R. S. Goldman, Appl. Phys. Lett. 110(24), 242102 (2017).
- ¹⁸D. E. Aspnes and A. A. Studna, Phys. Rev. B **27**(2), 985 (1983).
- ¹⁹A. Sakai and T. Tatsumi, Appl. Phys. Lett. **64**(1), 52 (1994).
- ²⁰O. Nakatsuka, S. Fujinami, T. Asano, T. Koyama, M. Kurosawa, M. Sakashita, H. Kishida, and S. Zaima, Jpn. J. Appl. Phys. 56(1S), 01AB05 (2017).
- ²¹C. A. Stephenson, M. Gillett-Kunnath, W. A. O'Brien, R. Kudrawiec, and M. A. Wistey, Crystals 6, 159 (2016).
- 22M. S. Reza, "Direct bandgap germanium for active silicon photonics application," Ph.D. dissertation (Material Science, Engineering, and Commercialization, Texas State University, San Marcos, TX, 2022), see https://hdl.handle.net/10877/
- $^{\mathbf{23}}$ G. Kresse and J. Furthmüller, Comput. Mater. Sci. $\mathbf{6}(1)$, 15 (1996).
- ²⁴P. E. Blöchl, Phys. Rev. B **50**(24), 17953 (1994).
- 25 T. Yamaha, K. Terasawa, H. Oda, M. Kurosawa, W. Takeuchi, N. Taoka, O. Nakatsuka, and S. Zaima, Jpn. J. Appl. Phys. 54(4S), 04DH08 (2015).
- ²⁶B. A. Weinstein and M. Cardona, Phys. Rev. B 7(6), 2545 (1973).
- ²⁷T. S. Perova, E. Kasper, M. Oehme, S. Cherevkov, and J. Schulze, J. Raman Spectrosc. 48(7), 993 (2017).
- ²⁸W. H. Weber, B.-K. Yang, and M. Krishnamurthy, Appl. Phys. Lett. **73**(5), 626 (1998).
- 29 M. Marton, M. Vojs, E. Zdravecká, M. Himmerlich, T. Haensel, S. Krischok, M. Kotlár, P. Michniak, M. Veselý, and R. Redhammer, J. Spectrosc. 2013, 1 (2013).
- 30 M. Mayer, AIP Conf. Proc. 475(1), 541 (1999).
- ⁵¹N. Bhargava, M. Coppinger, J. Prakash Gupta, L. Wielunski, and J. Kolodzey, Appl. Phys. Lett. **103**(4), 041908 (2013).
- $^{\bf 32}{\rm R}$. Matsutani, K. Sueoka, and E. Kamiyama, Phys. Status Solidi C 11(11-12), 1718 (2014).